



Maximal quantum Fisher information for phase estimation without initial parity

XU YU,¹ XIANG ZHAO,^{1,2} LUYI SHEN,^{1,3} YANYAN SHAO,⁴ JING LIU,^{4,5} AND XIAOGUANG WANG^{1,6}

¹Zhejiang Institute of Modern Physics, Department of Physics, Zhejiang University, Hangzhou 310027, China

²Department of Physics, ETH Zurich, 8049 Zurich, Switzerland

³Department of Engineer, Ecole Polytechnique, France

⁴MOE Key Laboratory of Fundamental Physical Quantities Measurement, Hubei Key Laboratory of Gravitation and Quantum Physics, School of Physics, Huazhong University of Science and Technology, Wuhan 430074, China

⁵liujingphys@hust.edu.cn

⁶xgwang@zimp.zju.edu.cn

Abstract: Mach-Zehnder interferometer is a common device in quantum phase estimation and the photon losses in it are an important issue for achieving a high phase accuracy. Here we thoroughly discuss the precision limit of the phase in the Mach-Zehnder interferometer with a coherent state and a superposition of coherent states as input states. By providing a general analytical expression of quantum Fisher information, the phase-matching condition and optimal initial parity are given. Especially, in the photon loss scenario, the sensitivity behaviors are analyzed and specific strategies are provided to restore the phase accuracies for symmetric and asymmetric losses.

© 2018 Optical Society of America under the terms of the [OSA Open Access Publishing Agreement](#)

OCIS codes: (270.0270) Quantum optics; (270.5585) Quantum information and processing.

References and links

1. V. Giovannetti, S. Lloyd, and L. Maccone, "Advances in quantum metrology," *Nat. Photonics* **5**, 222 (2011).
2. M. G. A. Paris, "Quantum estimation for quantum technology," *Int. J. Quantum Inform.* **7**, 125 (2009).
3. B. M. Escher, R. L. de Matos Filho, and L. Davidovich, "General framework for estimating the ultimate precision limit in noisy quantum-enhanced metrology," *Nat. Phys.* **7**, 406 (2011).
4. R. Demkowicz-Dobrzanski, J. Kolodynski, and M. Guta, "The elusive Heisenberg limit in quantum-enhanced metrology," *Nat. Commun.* **3**, 1063 (2012).
5. M. Tsang, "Quantum metrology with open dynamical systems," *New J. Phys.* **15**, 073005 (2013).
6. R. Demkowicz-Dobrzanski and L. Maccone, "Using entanglement against noise in quantum metrology," *Phys. Rev. Lett.* **113**, 250801 (2014).
7. H. Yuan and C.-H. F. Fung, "Optimal feedback scheme and universal time scaling for Hamiltonian parameter estimation," *Phys. Rev. Lett.* **115**, 110401 (2015).
8. H. Yuan, "Sequential feedback scheme outperforms the parallel scheme for Hamiltonian parameter estimation," *Phys. Rev. Lett.* **117**, 160801 (2016).
9. H. Yuan and C.-H. F. Fung, "Quantum parameter estimation with general dynamics," *Npj:Quantum Information* **3**, 14 (2017).
10. Y. Yao, L. Ge, X. Xiao, X. Wang, and C. P. Sun, "Multiple phase estimation for arbitrary pure states under white noise," *Phys. Rev. A* **90**, 062113 (2014).
11. G. Toth and I. Apellaniz, "Quantum metrology from a quantum information science perspective," *J. Phys. A: Math. Theor.* **47**, 424006 (2014).
12. J. Liu and H. Yuan, "Quantum parameter estimation with optimal control," *Phys. Rev. A* **96**, 012117 (2017).
13. J. Liu and H. Yuan, "Control-enhanced multiparameter quantum estimation," *Phys. Rev. A* **96**, 042114 (2017).
14. R. Schnabel, N. Mavalvala, D. E. McClelland, and P. K. Lam, "Quantum metrology for gravitational wave astronomy," *Nat. Commun.* **1**, 121 (2010).
15. M. J. Snadden, J. M. McGuirk, P. Bouyer, K. G. Haritos, and M. A. Kasevich, "Measurement of the Earth's gravity gradient with an atom interferometer-based gravity gradiometer," *Phys. Rev. Lett.* **81**, 971 (1998).
16. A. Peters, K. Y. Chung, and S. Chu, "Measurement of gravitational acceleration by dropping atoms," *Nature* **400**, 849-852 (1999).

17. S. D. Huver, C. F. Wildfeuer, and J. P. Dowling, "Entangled Fock states for robust quantum optical metrology, imaging, and sensing," *Phys. Rev. A* **78**, 063828 (2008).
18. R. T. Glasser, H. Cable, J. P. Dowling, F. De Martini, F. Sciarrino, and C. Vitelli, "Entanglement-seeded, dual, optical parametric amplification: Applications to quantum imaging and metrology," *Phys. Rev. A* **78**, 012339 (2008).
19. Y. H. Shih, "Quantum imaging," *IEEE J. Sel. Top. Quantum Electron.* **13**, 1016 (2007).
20. R. W. Boyd and J. P. Dowling, "Quantum lithography: Status of the field," *Quantum Inf. Process.* **11**, 891 (2012).
21. M. A. Taylor and W. P. Bowen, "Quantum metrology and its application in biology," *Phys. Rep.* **615**, 1-59 (2016).
22. B. P. Abbott, (LIGO Scientific Collaboration and the Virgo Collaboration), "Observation of gravitational waves from a binary black hole merger," *Phys. Rev. Lett.* **116**, 061102 (2016).
23. S. Vitale, "Multiband gravitational-wave astronomy: parameter estimation and tests of general relativity with space- and ground-based detectors," *Phys. Rev. Lett.* **117**, 051102 (2016).
24. J. Luo, L.-S. Chen, H.-Z. Duan, Y.-G. Gong, S. Hu, J. Ji, Q. Liu, J. Mei, V. Milyukov, M. Sazhin, C.-G. Shao, V. T. Toth, H.-B. Tu, Y. Wang, Y. Wang, H.-C. Yeh, M.-S. Zhan, Y. Zhang, V. Zharov, and Z.-B. Zhou, "TianQin: a space-borne gravitational wave detector," *Class. Quant. Grav.* **33**, 035010 (2016).
25. C. M. Caves, "Quantum-mechanical noise in an interferometer," *Phys. Rev. D* **23**, 1693 (1981).
26. L. Pezze and A. Smerzi, "Mach-Zehnder interferometry at the Heisenberg limit with coherent and squeezed-vacuum light," *Phys. Rev. Lett.* **100**, 073601 (2008).
27. P. Liu, P. Wang, W. Yang, G. R. Jin, and C. P. Sun, "Fisher information of a squeezed-state interferometer with a finite photon-number resolution," *Phys. Rev. A* **95**, 023824 (2017).
28. P. Liu and G. R. Jin, "Ultimate phase estimation in a squeezed-state interferometer using photon counters with a finite number resolution," *J. Phys. A: Math. Theor.* **50**, 405303 (2017).
29. D. J. Wineland, J. J. Bollinger, W. M. Itano, and D. J. Heinzen, "Squeezed atomic states and projection noise in spectroscopy," *Phys. Rev. A* **50**, 67 (1994).
30. D. Leibfried, M. D. Barrett, T. Schaetz, J. Britton, J. Chiaverini, W. M. Itano, J. D. Jost, C. Langer, and D. J. Wineland, "Toward Heisenberg-limited spectroscopy with multiparticle entangled States," *Science* **304**, 1476 (2004).
31. P. C. Humphreys, M. Barbieri, A. Datta, and I. A. Walmsley, "Quantum enhanced multiple phase estimation," *Phys. Rev. Lett.* **111**, 070403 (2013).
32. J. Joo, W. J. Munro, and T. P. Spiller, "Quantum metrology with entangled coherent states," *Phys. Rev. Lett.* **107**, 083601 (2011).
33. J. Joo, K. Park, H. Jeong, W. J. Munro, K. Nemoto, and T. P. Spiller, "Quantum metrology for nonlinear phase shifts with entangled coherent states," *Phys. Rev. A* **86**, 043828 (2012).
34. J. Liu, X.-M. Lu, Z. Sun, and X. Wang, "Quantum multiparameter metrology with generalized entangled coherent state," *J. Phys. A: Math. Theor.* **49**, 115302 (2016).
35. Y. Israel, L. Cohen, X.-B. Song, J. Joo, H. S. Eisenberg, and Y. Silberberg, "Entangled coherent states by mixing squeezed vacuum and coherent light," arXiv:1707.01809.
36. B. C. Sanders, "Entangled coherent states," *Phys. Rev. A* **45**, 6811 (1992).
37. C. C. Gerry, "Generation of Schrödinger cats and entangled coherent states in the motion of a trapped ion by a dispersive interaction," *Phys. Rev. A* **55**, 2478 (1997).
38. C. C. Gerry and J. Mimih, "Heisenberg-limited interferometry with pair coherent states and parity measurements," *Phys. Rev. A* **82**, 013831 (2010).
39. J. J. Cooper, D. W. Hallwood, and J. A. Dunningham, "Entanglement-enhanced atomic gyroscope," *Phys. Rev. A* **81**, 043624 (2010).
40. L. Pezze and A. Smerzi, "Ultrasensitive two-mode interferometry with single-mode number squeezing," *Phys. Rev. Lett.* **110**, 163604 (2013).
41. C. W. Helstrom, *Quantum Detection and Estimation Theory* (Academic, 1976).
42. A. S. Holevo, *Probabilistic and Statistic Aspects of Quantum Theory* (North-Holland, 1982).
43. S. L. Braunstein and C. M. Caves, "Statistical distance and the geometry of quantum states," *Phys. Rev. Lett.* **72**, 3439 (1994).
44. V. Giovannetti, S. Lloyd, and L. Maccone, "Quantum metrology," *Phys. Rev. Lett.* **96**, 010401 (2006).
45. P. A. Knott, T. J. Proctor, Kae Nemoto, J. A. Dunningham and W. J. Munro, "Effect of multimode entanglement on lossy optical quantum metrology," *Phys. Rev. A* **90**, 033846 (2014).
46. M. Takeoka, K. P. Seshadreesan, C. You, S. Izumi, and J. P. Dowling, "Fundamental precision limit of a Mach-Zehnder interferometric sensor when one of the inputs is the vacuum," *Phys. Rev. A* **96**, 052118 (2017).
47. R. Demkowicz-Dobrzanski, U. Dorner, B. J. Smith, J. S. Lundeen, W. Wasilewski, K. Banaszek, and I. A. Walmsley, "Quantum phase estimation with lossy interferometers," *Phys. Rev. A* **80**, 013825 (2009).
48. N. Gkortsilas, J. J. Cooper, and J. A. Dunningham, "Measuring a completely unknown phase with sub-shot-noise precision in the presence of loss," *Phys. Rev. A* **85**, 063827 (2012).
49. Y. M. Zhang, X. W. Li, W. Yang, and G. R. Jin, "Quantum Fisher information of entangled coherent states in the presence of photon loss," *Phys. Rev. A* **88**, 043832 (2013).
50. J. Liu, X. Jing, W. Zhong, and X. Wang, "Quantum Fisher information for density matrices with arbitrary ranks," *Commun. Theor. Phys.* **61**, 45–50 (2014).
51. J. Liu, H.-N. Xiong, F. Song, and X. Wang, "Fidelity susceptibility and quantum Fisher information for density operators with arbitrary ranks," *Physica A* **410**, 167–173 (2014).

52. S. Pang and T. A. Brun, "Quantum metrology for a general Hamiltonian parameter," *Phys. Rev. A* **90**, 022117 (2014).
53. Z. Jiang, "Quantum Fisher information for states in exponential form," *Phys. Rev. A* **89**, 032128 (2014).
54. J. Liu, X.-X. Jing and X. Wang, "Quantum metrology with unitary parametrization processes," *Sci. Rep.* **5**, 8565 (2015).
55. J. Liu, J. Chen, X.-X. Jing, and X. Wang, "Quantum Fisher information and symmetric logarithmic derivative via anti-commutators," *J. Phys. A: Math. Theor.* **49**, 275302 (2016).
56. B. Yurke, S. L. McCall and J. R. Klauder, "SU(2) and SU(1,1) interferometers," *Phys. Rev. A* **33**, 4033 (1986).
57. J. Liu, X. Jing and X. Wang, "Phase-matching condition for enhancement of phase sensitivity in quantum metrology," *Phys. Rev. A* **88**, 042316 (2013).
58. M. Jarzyna and R. Demkowicz-Dobrzanski, "True precision limits in quantum metrology," *New J. Phys.* **17**, 013010 (2015).
59. R. Demkowicz-Dobrzanski, M. Jarzyna, and J. Kolodynski, "Chapter four-Quantum limits in optical interferometry," *Progress in Optics*, **60**, 345–435 (2015).

1. Introduction

Quantum metrology, an emerging quantum technology, has been widely studied [1–13] and applied in various scientific tasks in recent years, including the detection of gravitational wave [14–16], quantum imaging [17–20] and even biology science [21]. Quantum phase estimation via interferometers is an important topic in quantum metrology. A successful example of phase estimation with interferometers is the Laser Interferometer Gravitational-Wave Observatory (LIGO), which has already caught the signal of gravitational waves [22] in 2015. Another two on-going projects LISA [23] and TianQin [24] are also based on the orbital optical interferometers. Hence, the study of optical phase estimation, especially quantum phase estimation, will definitely promote the technological development in these fields, and may even breed the next-generation detectors for gravitational waves and dark matters.

A $\mathfrak{su}(2)$ interferometer can be constructed via a Mach-Zehnder interferometer, which typically consists of two beam splitters and one phase shift in one arm, as shown in Fig. 1. Since Caves found the effects of vacuum fluctuation to the phase accuracy in Mach-Zehnder interferometers [25], various types of input states have been discussed, including squeezed state [25–28], NOON state [29–31], entangled coherent state [32–38], BAT state [39], and number squeezed state [40].

A powerful theoretical tool in quantum parameter estimation to depict the precision limit is the quantum Cramér-Rao bound, which is $\delta\hat{\phi} \geq 1/\sqrt{\mu F}$ [41–44]. Here $\delta\hat{\phi}$ is the standard deviation of parameter ϕ with unbiased estimator $\hat{\phi}$, μ is the repeated number of experiments and F is the quantum Fisher information (QFI). The most useful resource in the Mach-Zehnder interferometer is the average photon number \bar{n} , of which the corresponding standard quantum limit for $\delta\hat{\phi}$ is $1/\sqrt{\bar{n}}$ and the Heisenberg limit (or Heisenberg scaling) is $1/\bar{n}$.

Noise is the major obstacle for obtaining high precision result in quantum parameter estimation. For a large-scale, especially an in-orbit quantum interferometer (in the size of LISA and TianQin), the photon losses between the satellites could be an important issue for a high phase sensitivity. Therefore, fully understanding on the sensitivity behaviors under photon losses in the interferometer could help to restore a high precision as required. Many lossy scenarios with different input states have been discussed in the literature [32, 33, 45–48]. It is common to simulate the photon losses with fictitious beam splitters in theory, as shown in Fig. 1. In this paper, we discuss the precision limit of a Mach-Zehnder interferometer with a coherent state and a superposition of coherent states as the input states. Both perfect and imperfect (with photon losses) scenarios are considered and the analytical expression of QFI is provided. With this expression, the phase-matching condition (PMC) of the input states and the optimal QFI are calculated. For the imperfect scenario, symmetric and asymmetric losses are both studied and corresponding strategies to restore the accuracy are provided.

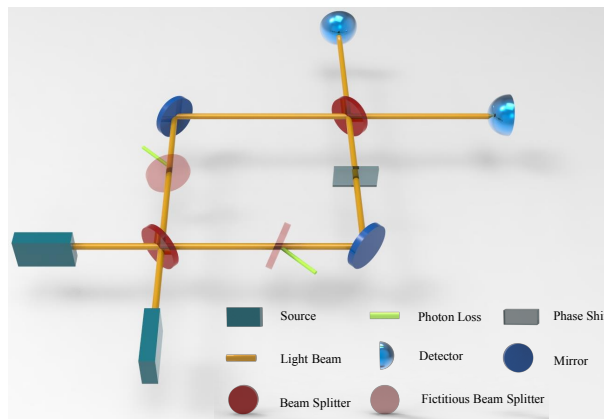


Fig. 1. Schematic of an Mach-Zehnder Interferometer. The input ports are labeled as A and B. The photon losses in the interferometer are simulated with two fictitious beam splitters, with corresponding operators $B_{AC}^{T_1}$ and $B_{BD}^{T_2}$. Here C and D are fictitious ports and T_1, T_2 are transmission rates. No photon losses exist for $T_1 = T_2 = 1$.

2. Preliminary knowledge

The quantum Fisher information (QFI) for a parameter ϕ is defined as $F := \text{Tr}(\rho_\phi L^2)$, where ρ_ϕ is the parameterized state and L is the symmetric logarithmic derivative operator satisfying $\partial_\phi \rho_\phi = \frac{1}{2}(L\rho_\phi + \rho_\phi L)$. Several methods for the calculation of QFI have been developed in recent years [49–55]. Utilizing the spectral decomposition $\rho_\phi = \sum_{i=1}^M p_i |\psi_i\rangle\langle\psi_i|$, with M , p_i and $|\psi_i\rangle$ the dimension of the support for the matrix, the eigenvalues and eigenstates of ρ_ϕ , the QFI can be expressed by [49–51]:

$$F = \sum_{i=1}^M \frac{(\partial_\phi p_i)^2}{p_i} + \sum_{i=1}^M 4p_i \langle \partial_\phi \psi_i | \partial_\phi \psi_i \rangle - \sum_{i,j=1}^M \frac{8p_i p_j}{p_i + p_j} |\langle \psi_i | \partial_\phi \psi_j \rangle|^2. \quad (1)$$

For the unitary parameterization process $\rho_\phi = e^{-iH\phi} \rho e^{iH\phi}$, with H a Hermitian operator, the expression of the QFI reduces to

$$F = \sum_{i=1}^M 4p_i \langle \psi_i | H^2 | \psi_i \rangle - \sum_{i,j=1}^M \frac{8p_i p_j}{p_i + p_j} |\langle \psi_i | H | \psi_j \rangle|^2. \quad (2)$$

Furthermore, for a pure state $|\psi_\phi\rangle$, it reduces to

$$F = 4 \left(\langle \psi_\phi | H^2 | \psi_\phi \rangle - |\langle \psi_\phi | H | \psi_\phi \rangle|^2 \right). \quad (3)$$

In this paper, we focus on the phase estimation in the Mach-Zehnder interferometer, as shown in Fig. 1. The interferometer consists of two beam splitters and a phase shift. The two beam splitters are usually taken as 50:50 beam splitters, which in theory can be expressed by $B_x (\pm \frac{\pi}{2}) = \exp(\pm i \frac{\pi}{2} J_x^{\text{AB}})$. Here J_x^{AB} is a Schwinger operator defined as $J_x^{\text{AB}} = \frac{1}{2}(a^\dagger b + b^\dagger a)$ with a (b) the annihilation operator for port A (B) and a^\dagger (b^\dagger) the corresponding creation operators. The other two Schwinger operators are $J_y^{\text{AB}} = \frac{1}{2i}(a^\dagger b - b^\dagger a)$ and $J_z^{\text{AB}} = \frac{1}{2}(a^\dagger a - b^\dagger b)$. The Schwinger operators satisfy the $\mathfrak{su}(2)$ algebra. The operator for the phase shift is $U(\phi) = \exp(i\phi J_z^{\text{AB}})$. For a perfect Mach-Zehnder interferometer, one expression of the entire setup can be written as the unitary operator below [56]

$$U_{\text{MZ}} = B_x \left(-\frac{\pi}{2} \right) U(\phi) B_x \left(\frac{\pi}{2} \right) = \exp \left(-i\phi J_y^{\text{AB}} \right). \quad (4)$$

The photon loss in the interferometer is usually depicted via fictitious beam splitters in theory. The effect of a general beam splitter for ports X and Y in quantum optics can be written as $B_{XY}^T = \exp(i2\arccos\sqrt{T}J_x^{XY})$ [47,48], where T is the transmission rate. When $T = 1$ ($T = 0$), all photons are transmitted (reflected). In many scenarios, especially in the large-scale interferometers, the optical path length is long and the dispersion of light spot is inevitable during the propagation, which will cause photon losses at the second beam splitter. In this paper, ports A and B are input ports of the interferometer and ports C and D are the fictitious ports for photon losses. The effects of fictitious beam splitters are expressed by $B_{AC}^{T_1}$ and $B_{BD}^{T_2}$. The arm with respect to port A (B) has no photon losses for $T_1 = 1$ ($T_2 = 1$) and all photons are lost for $T_1 = 0$ ($T_2 = 0$).

3. Perfect interferometer

For the perfect interferometer and with a pure input state, the QFI can be directly obtained by substituting Eq. (4) into Eq. (3), which is

$$F = \left(2\bar{n}_A\bar{n}_B + \bar{n}_A + \bar{n}_B - 2|\langle a \rangle|^2|\langle b \rangle|^2\right) - 2\text{Re}\left(\langle a^2 \rangle\langle b^{\dagger 2} \rangle - \langle a \rangle^2\langle b^{\dagger} \rangle^2\right),$$

where $\text{Re}(\cdot)$ represent the real part and $\bar{n}_A = \langle a^{\dagger}a \rangle$, $\bar{n}_B = \langle b^{\dagger}b \rangle$ are the average photon numbers for both arms.

Taking a coherent state $|\beta\rangle$ as the input state for port A, and an arbitrary pure state $|\psi\rangle$ for port B, $\bar{n}_A = |\langle a \rangle|^2 = |\beta|^2$. The QFI then reads

$$F = 2\bar{n}_A \left(\bar{n}_B - |\langle b \rangle|^2 \right) + \bar{n}_A + \bar{n}_B - 2\text{Re} \left[\beta^2 \left(\langle b^{\dagger 2} \rangle - \langle b^{\dagger} \rangle^2 \right) \right]. \quad (5)$$

For a given $|\psi\rangle$, F only depends on the value of β , and the PMC optimizing the QFI is

$$\left| \text{Arg} \left(\beta^2 \right) - \text{Arg} \left(\langle b^2 \rangle - \langle b \rangle^2 \right) \right| = \pi, \quad (6)$$

where $\text{Arg}(\cdot)$ is the argument. With this condition, the optimal QFI can be calculated as

$$F_m = 2\bar{n}_A \left(\bar{n}_B - |\langle b \rangle|^2 + |\langle b^2 \rangle - \langle b \rangle^2| \right) + \bar{n}_A + \bar{n}_B. \quad (7)$$

Next we take the input state in port B as the superposition of two coherent states $|\alpha\rangle$ and $|-\alpha\rangle$, i.e.,

$$|\psi\rangle = N_\alpha (|\alpha\rangle + e^{i\Theta} |-\alpha\rangle), \quad (8)$$

where $\Theta \in [0, 2\pi]$ is the relative phase and the normalization factor N_α reads $N_\alpha = (2 + 2e^{-2|\alpha|^2} \cos \Theta)^{-1/2}$. In the following we denote $\beta = |\beta|e^{i\Phi_A}$, $\alpha = |\alpha|e^{i\Phi_B}$, with Φ_A , Φ_B the arguments of β and α . Through some straightforward calculation, the PMC for optimal QFI can be written as

$$|\Phi_A - \Phi_B| = \frac{\pi}{2}, \quad (9)$$

which coincides with the case that using a coherent superposition state in port B [57], namely, the relative phase Θ doesn't affect the PMC. Under this condition, the maximal QFI reads

$$F_m = \bar{n}_A(2|\alpha|^2 + 1) + \bar{n}_B(2\bar{n}_A + 1). \quad (10)$$

Utilizing the equations $\bar{n}_A = |\beta|^2$ and $\bar{n}_B = 2N_\alpha^2|\alpha|^2(1 - e^{-2|\alpha|^2} \cos \Theta)$, the maximal F_m can be reached when $\Theta = \pi$, which means taking into account the PMC, the QFI can be further improved with an initial odd parity of $|\psi\rangle$.

Now we compare F_m with Heisenberg scaling. Denote $\bar{n} = \bar{n}_A + \bar{n}_B$ as the average total input photon number, Eq. (10) can then be rewritten into $F_m = \bar{n} + 2\bar{n}_A(\bar{n}_B + |\alpha|^2)$. For a large $|\alpha|$,

$\bar{n}_B \approx |\alpha|^2$, $F_m \approx \bar{n} + 4\bar{n}_A\bar{n}_B = \bar{n} + \bar{n}^2 - (\delta\bar{n})^2$ with $\delta\bar{n} = \bar{n}_A - \bar{n}_B$ the photon difference between two ports. When $\delta\bar{n}$ is small (compared to \bar{n}), F_m reduces to $\bar{n} + \bar{n}^2$, i.e., $F_m \propto \bar{n}^2$, indicating the QFI under PMC can reach the Heisenberg scaling even no initial parity exists in $|\psi\rangle$. Furthermore, it can be found that

$$F_m \leq \langle \hat{n}^2 \rangle, \quad (11)$$

which can be proved as $F_m - \langle \hat{n}^2 \rangle = -(|\beta|^2 - |\alpha|^2)^2 \leq 0$. Here we used $\langle \hat{n}^2 \rangle = \bar{n}_A^2 + 2\bar{n}_A\bar{n}_B + \bar{n} + |\alpha|^4$. This upper bound can be achieved for $|\beta| = |\alpha|$. To satisfy this condition, one can take $\beta = \alpha e^{i(\Phi + \frac{\pi}{2})}$ with Φ the relative phase between the values of α and β , hence the total input state is $N_\alpha |\alpha e^{i(\Phi + \frac{\pi}{2})}\rangle_A \otimes (|\alpha\rangle_B + e^{i\Theta}|-\alpha\rangle_B)$. According to Eq. (6), the PMC is $\Phi = 0$ or π , which is indeed independent of Θ .

4. Imperfect interferometer

For an imperfect Mach-Zehnder interferometer, the total effect cannot be treated as an unitary operation. As discussed in the previous section, the photon losses are simulated with beam splitters $B_{AC}^{T_1} = \exp[i2 \arccos \sqrt{T_1} J_x^{AC}]$ and $B_{BD}^{T_2} = \exp[i2 \arccos \sqrt{T_2} J_x^{BD}]$. Here $J_x^{AC} = \frac{1}{2}(a^\dagger c + c^\dagger a)$, $J_x^{BD} = \frac{1}{2}(b^\dagger d + d^\dagger b)$ with c (c^\dagger) and d (d^\dagger) the annihilation (creation) operators of the fictitious lossy ports C and D. We take the total input state as

$$N_\alpha |\alpha e^{i(\Phi + \frac{\pi}{2})}\rangle_A (|\alpha\rangle_B + e^{i\Theta}|-\alpha\rangle_B). \quad (12)$$

After the photon losses, the state becomes a mixed state, which can be written as (the basis information and detailed calculation can be found in the appendix)

$$\rho_1 = N_\alpha^2 \begin{pmatrix} 1 + p_t^2 + 2e^{-2|\alpha|^2} \cos \Theta & \sqrt{1 - p_t^2} (p_t + p_r e^{-i\Theta}) e^{i|\alpha|^2 \delta T \sin \Phi} \\ \sqrt{1 - p_t^2} (p_t + p_r e^{i\Theta}) e^{-i|\alpha|^2 \delta T \sin \Phi} & 1 - p_t^2 \end{pmatrix}, \quad (13)$$

where $p_t = e^{-|\alpha|^2 T}$, $p_r = e^{-|\alpha|^2 R}$ and $T = T_1 + T_2$ is the total transmission rate of the photon losses, $R = 2 - T$ is the total reflection rate, $\delta T = T_1 - T_2$ is the transmission difference between the two ports. Since the last 50:50 beam splitter in the interferometer does not affect the value of QFI as it is independent of θ , the total effect of the lossy interferometer is equivalent to perform the phase shift transform $U(\theta)$ to ρ_1 . Denote the eigenvalues and eigenstates of ρ_1 as λ_\pm and $|\lambda_\pm\rangle$, respectively, the QFI can be expressed by

$$F = \sum_{i=\pm} 4\lambda_i \langle \lambda_i | (J_z^{AB})^2 | \lambda_i \rangle - \sum_{i,j=\pm} \frac{8\lambda_i \lambda_j}{\lambda_i + \lambda_j} |\langle \lambda_i | J_z^{AB} | \lambda_j \rangle|^2. \quad (14)$$

Utilizing the expressions of λ_\pm and $|\lambda_\pm\rangle$ (given in the appendix) and through some tedious calculation, the specific expression of QFI can be written as

$$\begin{aligned} F = & 2(\delta T)^2 \frac{N_\alpha^6 |\alpha|^4 p_t}{\Delta(1 - p_t^2)} \left[4p_r(p_r + p_t \cos \Theta)(p_t + p_r \cos \Theta) - \frac{\Delta}{N_\alpha^4} p_t \right] \\ & - 16(\delta T)^2 \frac{N_\alpha^8}{\Delta} |\alpha|^4 (1 - p_r^2) e^{-4|\alpha|^2} \sin^2 \Theta + 2\delta T N_\alpha^2 |\alpha|^2 e^{-2|\alpha|^2} (4TN_\alpha^2 |\alpha|^2 - 1) \sin \Theta \sin \Phi \\ & + 2T^2 |\alpha|^4 N_\alpha^2 \left[1 - 2N_\alpha^2 (1 - p_r^2) - \left(\frac{\Delta}{2N_\alpha^2} + 2N_\alpha^2 e^{-4|\alpha|^2} \sin^2 \Theta \right) \sin^2 \Phi \right] + 2TN_\alpha^2 |\alpha|^2. \end{aligned} \quad (15)$$

where $\Delta = 1 - 4 \det \rho_1 = 1 - 4N_\alpha^4(1 - p_r^2)(1 - p_t^2)$. Next we will discuss the PMCs and maximum QFIs for symmetric and asymmetric losses scenarios.

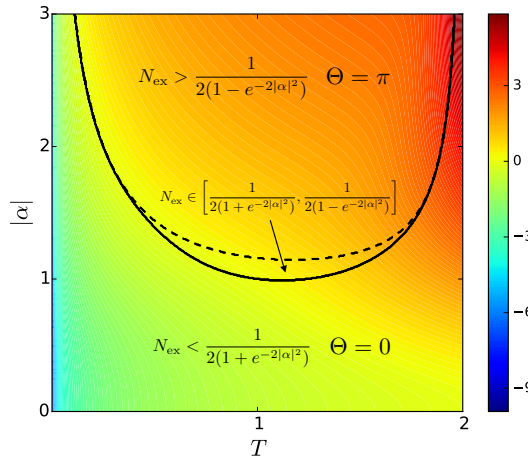


Fig. 2. The values of $\max_{\Theta} F_m$ as a function of T and $|\alpha|$. The areas below the solid black line, above the dashed black line and between these lines represent the regimes that $N_{ex} < (2 + 2e^{-2|\alpha|^2})^{-1}$ (optimal Θ is 0), $N_{ex} > (2 - 2e^{-2|\alpha|^2})^{-1}$ (optimal Θ is π) and $N_{ex} \in [(2 + 2e^{-2|\alpha|^2})^{-1}, (2 - 2e^{-2|\alpha|^2})^{-1}]$. The PMC here is $\Phi = 0, \pi$. $\max_{\Theta} F_m$ takes the logarithmic values in the figure.

4.1. Symmetric losses

We first consider the symmetric losses case. In this case, the transmission rate in both arms are equivalent, i.e., $\delta T = 0$. With this condition, the QFI in Eq. (15) reduces to

$$F = 2T^2|\alpha|^4N_\alpha^2 \left[1 - 2N_\alpha^2(1 - p_r^2) - \left(\frac{\Delta}{2N_\alpha^2} + 2N_\alpha^2e^{-4|\alpha|^2} \sin^2 \Theta \right) \sin^2 \Phi \right] + 2TN_\alpha^2|\alpha|^2. \quad (16)$$

To maximize F , the corresponding PMC is $\Phi = 0$ or π , which is the same with lossless case. Utilizing the PMC, F_m is in the form

$$F_m = 2TN_\alpha^2|\alpha|^2 \{ 1 + T|\alpha|^2 [1 - 2N_\alpha^2(1 - p_r^2)] \}. \quad (17)$$

Recall the fact that N_α is a function of Θ , F_m can be further improved by optimizing Θ . Utilizing the equation $\frac{\partial F_m}{\partial N_\alpha^2} = 0$, it can be found the extremal value of F_m is reached at

$$N_\alpha^2 = N_{ex} := \frac{1 + T|\alpha|^2}{4T|\alpha|^2(1 - p_r^2)} \quad (18)$$

and due to the fact $\frac{\partial^2 F_m}{(\partial N_\alpha^2)^2} < 0$, this extremal value is the maximum value. One may notice that N_α^2 is a bounded function with respect to Θ ,

$$N_\alpha^2 \in \left[\frac{1}{2(1 + e^{-2|\alpha|^2})}, \frac{1}{2(1 - e^{-2|\alpha|^2})} \right], \quad (19)$$

where the lower and upper bounds of N_α^2 can be attained at $\Theta = 0$ and π , respectively. To obtain the actual maximum value of F_m , whether N_{ex} locates in above regime needs to be considered. The specific relation between N_{ex} and above regime is shown in Fig. 2. The areas below the solid black line and above the dashed black line represent the regimes that $N_{ex} < (2 + 2e^{-2|\alpha|^2})^{-1}$ and

$N_{\text{ex}} > (2 - 2e^{-2|\alpha|^2})^{-1}$, respectively. The area between these lines represents the regime that $N_{\text{ex}} \in [(2 + 2e^{-2|\alpha|^2})^{-1}, (2 - 2e^{-2|\alpha|^2})^{-1}]$.

In the regime that $N_{\text{ex}} > (2 - 2e^{-2|\alpha|^2})^{-1}$, N_{ex} is not attainable and the maximum value of F_m with respect to Θ is obtained at $\Theta = \pi$, namely, an initial odd parity is required. In this case,

$$\max_{\Theta} F_m = \frac{T|\alpha|^2}{1 - e^{-2|\alpha|^2}} \left[1 + T|\alpha|^2 \left(1 - \frac{1 - e^{-2|\alpha|^2 R}}{1 - e^{-2|\alpha|^2}} \right) \right]. \quad (20)$$

Similarly, in the regime that $N_{\text{ex}} < (2 + 2e^{-2|\alpha|^2})^{-1}$, N_{ex} is also not attainable and the maximum value of F_m with respect to Θ is obtained at $\Theta = 0$, namely, an initial even parity is required for optimal F_m . In this case,

$$\max_{\Theta} F_m = \frac{T|\alpha|^2}{1 + e^{-2|\alpha|^2}} \left[1 + T|\alpha|^2 \left(1 - \frac{1 - e^{-2|\alpha|^2 R}}{1 + e^{-2|\alpha|^2}} \right) \right]. \quad (21)$$

In the regime that $N_{\text{ex}} \in [(2 + 2e^{-2|\alpha|^2})^{-1}, (2 - 2e^{-2|\alpha|^2})^{-1}]$, N_{ex} is reachable and the maximum F_m can be attained at $N_{\alpha}^2 = N_{\text{ex}}$. The maximum F_m reads

$$\max_{\Theta} F_m = \frac{(1 + T|\alpha|^2)^2}{4(1 - e^{-2|\alpha|^2 R})}. \quad (22)$$

The optimal Θ satisfies the following equation

$$\cos \Theta = \frac{-2T|\alpha|^2 e^{-2|\alpha|^2(1-T)} + (T|\alpha|^2 - 1)e^{2|\alpha|^2}}{1 + T|\alpha|^2}. \quad (23)$$

In this regime, the optimal Θ relies on the values of T , $|\alpha|$ and both odd and even input states are non-optimal.

From the lines shown in Fig. 2, it can be seen the area between the lines is small, which means for most values of T and $|\alpha|$, N_{ex} is out of the regime $[(2 + 2e^{-2|\alpha|^2})^{-1}, (2 - 2e^{-2|\alpha|^2})^{-1}]$, and initial parity will benefit the precision limit. Besides, though the PMC here is not changed compared to the lossless scenario, the maximum F_m with respect to Θ is different for different parameter regimes as discussed above. However, in all regimes, increasing the intensity of initial state always benefits the precision limit, as shown in Fig. 2. Thus, for an intermediate photon loss rate, the best strategy to hold the precision limit is to use a high intensity odd state as the input state. However, for a low photon loss rate, one should be more careful since the increasing of the intensity may require a changed parity for optimal precision limit. And to keep the odd parity to be optimal, a higher intensity is required with the decrease of the photon loss rate (the increase of the transmission rate T).

4.2. Asymmetric losses

For asymmetric losses scenario, $\delta T \neq 0$. To find the PMC, the derivative of QFI on $\sin \Phi$ needs to be calculated. Based on Eq. (15), it is

$$\frac{\partial F}{\partial \sin \Phi} = -2\delta T N_{\alpha}^2 |\alpha|^2 e^{-2|\alpha|^2} \sin \Theta (1 - 4TN_{\alpha}^2 |\alpha|^2) - 2T^2 |\alpha|^4 (\Delta + 4N_{\alpha}^4 e^{-4|\alpha|^2} \sin^2 \Theta) \sin \Phi. \quad (24)$$

Due to the fact $\frac{\partial^2 F}{\partial \sin \Phi^2} < 0$, the solution for above equation gives the maximum value of QFI, i.e., the optimal Φ needs to satisfy

$$\sin \Phi = N'_{\text{ex}} := \frac{N_{\alpha}^2 (4TN_{\alpha}^2 |\alpha|^2 - 1) \sin \Theta}{T^2 |\alpha|^2 (\Delta e^{2|\alpha|^2} + 4N_{\alpha}^4 e^{-2|\alpha|^2} \sin^2 \Theta)} \delta T. \quad (25)$$

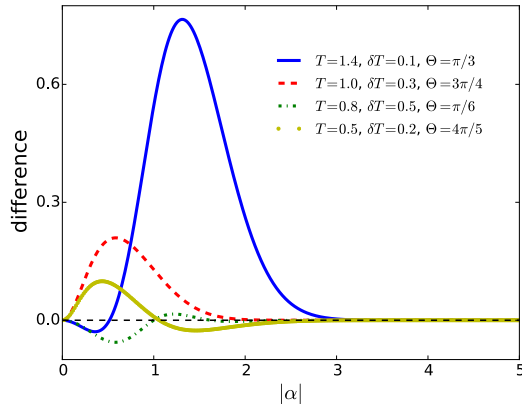


Fig. 3. The difference between Eq. (15) and $T|\alpha|^2$ under the PMC $\Phi = 0$. The expression $T|\alpha|^2$ is a good approximation from $|\alpha| \approx 3$ for the coefficients values in the figure. A larger transmission rate T requires a larger $|\alpha|$ for this approximation.

The solution for this equation relies on the values of Θ . However, similar to the symmetric scenario, $\sin \Phi$ is restrained in the regime $[-1, 1]$. Hence, when $N'_{\text{ex}} \in [-1, 1]$, the PMC is the solution for above equation, especially, if the input state is an even state, i.e., $\Theta = 0$, the PMC then reads $\Phi = 0$. For case that $N'_{\text{ex}} > 1$, the PMC is $\Phi = \pi/2$, and for $N'_{\text{ex}} < -1$, the PMC is $\Phi = 3\pi/2$.

For a low intensity input ($|\alpha|$ is very small), $N'_{\text{ex}} \approx \frac{1}{2T} \tan \frac{\Theta}{2} - \frac{\sin \Theta \delta T}{4T^2 |\alpha|^2}$. Its relation between the regime $[-1, 1]$ highly relies on the value of Θ and the sign of δT , indicating no constant PMC exists. A more concerned case is with a high intensity input. In this case, $N'^2_{\alpha} \approx 1/2$ and $\Delta e^{2|\alpha|^2} \approx e^{2|\alpha|^2(1-T)} + e^{2|\alpha|^2(1-R)}$. Since $1-T$ and $1-R$ always take different signs as $T+R=2$, $\Delta e^{2|\alpha|^2}$ is very large here. Thus, N'_{ex} approximates to zero. Based on Eq. (25), the PMC here is $\Phi \approx 0$ or π . Namely, for an asymmetric loss scenario with a high enough intensity input, the PMC can still be independent of Θ and the transmission rates. Another benefit of this PMC is that F_m is insensitive to the sign of δT (since it only exists together with $\sin \Phi$), i.e., the information of which path has a more severe leak is not required here. Taking this PMC ($\Phi = 0, \pi$), F_m approximates to

$$F_m \approx T|\alpha|^2, \quad (26)$$

which is independent of Θ . Figure 3 shows the difference between Eq. (15) and $T|\alpha|^2$ for different parameter settings. Generally, a larger transmission rate requires a larger $|\alpha|$ to converge to $T|\alpha|^2$. However, for the specific parameters given in the figure, all F_m converge before around $|\alpha| = 3.0$, which means $T|\alpha|^2$ is a very good approximation here for $|\alpha| > 3.0$ regardless the values of T , δT and Θ . Thus, for the asymmetric losses scenario, one efficient strategy to restore the precision limit is inputting a high intensity state satisfying the PMC.

4.3. The scaling

The average total photon number \bar{n} for the input state in Eq. (12) is

$$\bar{n} = \frac{2|\alpha|^2}{1 + e^{-2|\alpha|^2} \cos \Theta}. \quad (27)$$

For a large $|\alpha|$, $\bar{n} \approx 2|\alpha|^2$. In the symmetric losses scenario, Eqs. (20) and (21) indicate $\max_{\Theta} F_m \propto \bar{n}$ for a nonzero R , which means it can only reach the standard quantum limit in these regime. For

Eq. (22), $\max_{\Theta} F_m \propto \bar{n}^2$, i.e., it can still attain the Heisenberg scaling, however, the allowed value of $|\alpha|$ in this regime (shown in Fig. 2) is very limited, and the absolute value of $\max_{\Theta} F_m$ is still worse than Eq. (20) with a large $|\alpha|$. Therefore, the scaling of $\max_{\Theta} F_m$ for symmetric losses can only provide a precision at the standard quantum limit. For asymmetric losses scenario, taking into account the PMC, F_m approximates to $T|\alpha|^2$ for high intensity state, i.e., proportional to \bar{n} , the standard quantum limit. This phenomenon coincides with some other cases that the precision limit is bounded by the standard quantum limit when local noise exists [3, 4, 49, 58, 59].

5. Conclusion

This paper focuses on the phase estimation of a $\mathfrak{su}(2)$ Mach-Zehnder interferometer, in which the unknown parameter ϕ is encoded by a phase shift in one arm. The input states is a coherent state $|\beta\rangle$ and a superposition state of coherent states $N_\alpha(|\alpha\rangle + e^{i\Theta}|-\alpha\rangle)$. Both perfect and imperfect scenarios are considered. For the perfect scenario, the phase-matching condition to optimize the QFI is given. With this condition, the QFI can be further improved by taking $\Theta = \pi$, i.e., using an odd parity state (cat state). For the imperfect scenario, the photon losses in both arms are simulated by two fictitious beam splitters. The general analytical expression of QFI are provided, as well as the phase-matching condition and optimal Θ to maximize QFI. In the symmetric losses case, the phase-matching condition is unchanged compared to the lossless case. Furthermore, there exists a small parameter regime for total transmission rate T and $|\alpha|$ that optimal Θ is sensitive to them. To avoid this regime, one strategy is using a high intensity input state, of which the precision limit is at the standard quantum limit. However, it should be noticed that for a large T , increasing the intensity may requires the change of parity from even to odd in the mean time, and to keep the odd parity as the optimal one, a higher intensity is required with the decrease of the photon loss rate (increase of T). In the asymmetric losses case, taking the approximated phase-matching condition, an efficient strategy to avoid the sensitivity of maximum QFI on Θ and restore the sensitivity is also using the a high intensity input state satisfying the PMC.

Appendix: Derivation of QFI for imperfect interferometer

The input state we choose in this paper is

$$|\psi_{in}\rangle = |\alpha e^{i(\Phi+\frac{\pi}{2})}\rangle \otimes N_\alpha(|\alpha\rangle + e^{i\Theta}|-\alpha\rangle). \quad (28)$$

For the first 50:50 beam splitter, the state becomes $|\psi_0\rangle = B_x(\frac{\pi}{2})|\psi_{in}\rangle$. Utilizing the formula

$$B_x^T |\alpha\rangle_A |\beta\rangle_{A'} = \left| \alpha \sqrt{T} + i \beta \sqrt{1-T} \right\rangle_A \left| \beta \sqrt{T} + i \alpha \sqrt{1-T} \right\rangle_{A'}, \quad (29)$$

where $B_x^T = \exp(i2 \arccos T J_x^{AA'})$ and being aware of the fact $T = 1/2$ for 50:50 beam splitter, $|\psi_0\rangle$ can be written as

$$|\psi_0\rangle = N_\alpha \left(|if_+\rangle_A |f_-\rangle_B + e^{i\Theta} |if_-\rangle_A |f_+\rangle_B \right), \quad (30)$$

where $f_\pm := \frac{\alpha}{\sqrt{2}}(1 \pm e^{i\Phi})$. Recall the fictitious beam splitters $B_{AC}^{T_1}, B_{BD}^{T_1}$ as $\exp(i2 \arccos \sqrt{T_1} J_x^{AC})$ and $\exp(i2 \arccos \sqrt{T_2} J_x^{BD})$, where C, D are labels of two fictitious output ports with c (c^\dagger) and d (d^\dagger) the annihilation (creation) operators and $J_x^{AC} = \frac{1}{2}(a^\dagger c + ac^\dagger)$, $J_x^{BD} = \frac{1}{2}(b^\dagger d + bd^\dagger)$. Assume the input states of the fictitious input ports are vacuum, and after the photon losses, the output state $|\psi_1\rangle$ can be written as

$$|\psi_1\rangle = N_\alpha \left(|\mathcal{A}\rangle |f_+ \sqrt{R_1}\rangle_C |f_- \sqrt{R_2}\rangle_D + e^{i\Theta} |\mathcal{B}\rangle |f_- \sqrt{R_1}\rangle_C |f_+ \sqrt{R_2}\rangle_D \right), \quad (31)$$

where $|\mathcal{A}\rangle := |if_+\sqrt{T_1}\rangle_A|f_-\sqrt{T_2}\rangle_B$ and $|\mathcal{B}\rangle := |-if_-\sqrt{T_1}\rangle_A|-f_+\sqrt{T_2}\rangle_B$. $R_1 = 1 - T_1$, $R_2 = 1 - T_2$ are the reflection rates. The reduced matrix can then be calculated as

$$\begin{aligned}\rho_1 &= \text{Tr}_{CD}(|\psi_1\rangle\langle\psi_1|) \\ &= N_\alpha^2 [|\mathcal{A}\rangle\langle\mathcal{A}| + |\mathcal{B}\rangle\langle\mathcal{B}| + p_r e^{i(|\alpha|^2 \delta T \sin \Phi - \Theta)} |\mathcal{A}\rangle\langle\mathcal{B}| + p_r e^{-i(|\alpha|^2 \delta T \sin \Phi - \Theta)} |\mathcal{B}\rangle\langle\mathcal{A}|],\end{aligned}\quad (32)$$

where $p_r = e^{-|\alpha|^2 R}$ with $\delta T = T_1 - T_2$ the transmission difference. Notice $|\mathcal{A}\rangle$ and $|\mathcal{B}\rangle$ are not orthogonal due to the fact $\langle\mathcal{A}|\mathcal{B}\rangle = p_t e^{i|\alpha|^2 \delta T \sin \Phi}$ with $p_t = e^{-|\alpha|^2 T}$ and $T = T_1 + T_2$ the total transmission rate.

Now we introduce an orthogonal basis $\{|\mathcal{A}\rangle, |\mathcal{A}_\perp\rangle\}$, where

$$|\mathcal{A}_\perp\rangle = \frac{1}{\sqrt{1-p_t^2}} (|\mathcal{B}\rangle - p_t e^{i|\alpha|^2 \delta T \sin \Phi} |\mathcal{A}\rangle). \quad (33)$$

In this basis, ρ_1 can be written as

$$\rho_1 = N_\alpha^2 \begin{pmatrix} 1 + p_t^2 + 2e^{-2|\alpha|^2} \cos \Theta & \sqrt{1-p_t^2} (p_t + p_r e^{-i\Theta}) e^{i|\alpha|^2 \delta T \sin \Phi} \\ \sqrt{1-p_t^2} (p_t + p_r e^{i\Theta}) e^{-i|\alpha|^2 \delta T \sin \Phi} & 1 - p_t^2 \end{pmatrix}, \quad (34)$$

The eigenvalues for this matrix are $\lambda_\pm = N_\alpha^2(1 \pm \sqrt{\Delta})/2$ and corresponding eigenstates $|\lambda_\pm\rangle$ are

$$|\lambda_\pm\rangle = \left(v_\pm \frac{p_t + p_r e^{-i\Theta}}{\sqrt{p_t^2 + p_r^2 + 2e^{-2|\alpha|^2} \cos \Theta}} \mp \frac{p_t v_\mp}{\sqrt{1-p_t^2}} \right) |\mathcal{A}\rangle \pm \frac{v_\mp e^{-i|\alpha|^2 \delta T \sin \Phi}}{\sqrt{1-p_t^2}} |\mathcal{B}\rangle, \quad (35)$$

where we have used the expression of $|\mathcal{A}_\perp\rangle$. The coefficients read

$$v_\pm = \frac{1}{\sqrt{2}} \sqrt{1 \pm \frac{p_t^2 + e^{-2|\alpha|^2} \cos \Theta}{\sqrt{\Delta}(1 + e^{-2|\alpha|^2} \cos \Theta)}}, \quad (36)$$

$$= \frac{1}{\sqrt{\Delta}} \sqrt{\frac{\Delta}{2} \pm \sqrt{\Delta} N_\alpha^2 (p_t^2 + e^{-2|\alpha|^2} \cos \Theta)}, \quad (37)$$

$$\Delta = 1 - 4 \det \rho_1. \quad (38)$$

Funding

National Key Research and Development Program of China (2017YFA0205700 and 2017YFA0304202); National Natural Science Foundation of China (NSFC) (11475146); Fundamental Research Funds for the Central Universities (2017FZA3005).

Acknowledgments

The authors thank X. Xiao and J. Chen for helpful discussions.

Disclosures

The authors declare that there are no conflicts of interest related to this article.